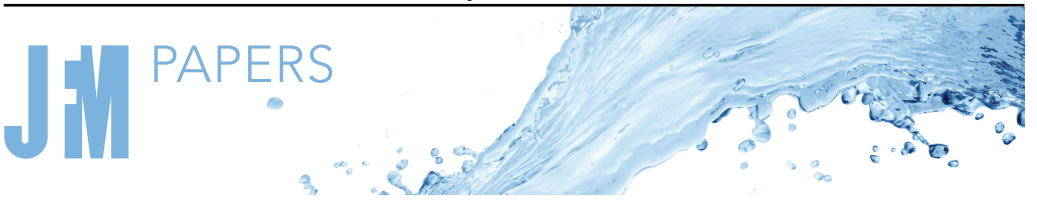
J. Fluid Mech. (2025), *vol.* 1009, A32, doi:10.1017/jfm.2025.156



Linear dynamics of over-expanded annular supersonic jets

Vincent Jaunet[1] **and Guillaume Lehnasch**[1]

[1]ISAE-ENSMA, Institut PPrime, Université de Poitiers, UPR-3346 CNRS, 1 Avenue Clement Ader, 86360 Chasseneuil-du-Poitou, France

Corresponding author: Vincent Jaunet, vincent.jaunet@ensma.fr

(Received 31 May 2024; revised 23 September 2024; accepted 18 January 2025)

This article delves into the dynamics of inviscid annular supersonic jets, akin to those exiting converging–diverging nozzles in over-expanded regimes. It focuses on the first azimuthal Fourier mode of flow fluctuations and examines their behaviour with varying mixing layer parameters and expansion regimes. The study reveals that two unstable Kelvin–Helmholtz waves exist in all cases, with the outer-layer wave being more unstable due to differences in the velocity gradient. The inner-layer wave is more sensitive to changes in base flow and extends beyond the jet, potentially contributing to nozzle resonances. The article also investigates upstream propagating guided-jet modes, which are found to be robust and not highly sensitive to changes in base flow, which makes them essential for understanding jet dynamics. A simplified model is used to obtain ideal base flows but with realistic shape in order to study the effects of varying nozzle pressure ratios on the dynamics of the waves supported by the jet.

Key words: supersonic flow, jets

1. Introduction

Thanks to the entry of new participants in the aerospace market, the interest in space access has recently been rekindled. This active competition, occurring in parallel with global environmental concerns, compels industries to develop launch systems that are more robust, efficient and cost-effective for deploying satellites into specific orbits. To mitigate expenses, reusable launchers and boosters have been designed, enabling their return and landing on the Earth's surface. During the descent and landing phases, a comprehensive understanding of the aerodynamics of the jet plume, exhausting at supersonic speed from the convergent–divergent nozzle, is imperative to avoid unintended mechanical stresses arising from uncontrolled pressure fluctuations. The start-up phase of the engines also confronts side-loads, which has motivated extensive research (see Nave & Coffey (1973);

© The Author(s), 2025. Published by Cambridge University Press.

https://doi.org/10.1017/jfm.2025.156 Published online by Cambridge University Press

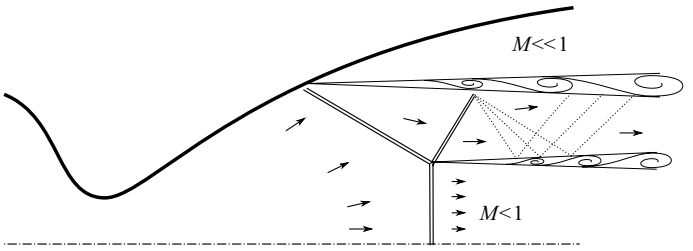


Figure 1. Illustration of TIC nozzle jet in a free shock separation regime.

Schmucker (1973*a*,*b*,*c*); Dumnov (1996); Deck & Nguyen (2004); Deck (2009) and the references therein for a subset of studies). Despite the fact that such issues may become even more critical during landing, where the jet may impinge on a flat surface, comprehensive and quantitative models for predicting unsteady pressure forces are still to be developed.

Resonances in jet flows originating from truncated ideal contour (TIC) nozzles, and operating within the free separation regime, have been observed within very narrow over-expansion ratio ranges (Baars *et al.* 2012; Jaunet *et al.* 2017; Martelli *et al.* 2020). Recent investigations have demonstrated that the associated pressure disturbances are likely to generate significant lateral off-axis forces that could lead to structural damage or even flight control problems (Bakulu *et al.* 2021). Despite the research efforts, no consensus on the origin of these resonances has yet emerged, and, among the various possible explanations, the role of vortex shed by the Mach disk (Martelli *et al.* 2020), the effect of the separated mixing layer impingement in the nozzle lip (Tarsia Morisco *et al.* 2023) or an internal screech feedback loop (Jaunet *et al.* 2017) have been hypothesised. The search for the necessary ingredient for a feedback loop to be sustained in these atypical flows is one of the motivations for this study.

In these particular flow regimes, the presence of Mach disks in the flow decelerates the central core of the jet, while a higher-velocity annular flow envelops this slower core, as depicted in figure 1. The mean flow thus comprises two co-annular jets, separated by a mixing layer emanating from the separation point and a slipline originating from the Mach disk triple point. The dynamics of these flow conditions have been shown to play a crucial role in the resonance mechanism and warrant more in-depth investigation to gain insights into the resonance process (Bakulu *et al.* 2021).

Axisymmetric bulk velocity profile jets (single jets) have garnered significant attention within the scientific community, in particular, to predict their acoustics (Jordan & Colonius 2013). Hence, substantial efforts have been dedicated to modelling the dynamics of these jets, employing linearised models, with the well-known tanh profile serving as a proxy for the jet's base flow (Michalke 1984). Supersonic jet flows have also been extensively studied, and numerous dynamical models have been developed to understand their dynamics (Tam & Hu 1989), noise characteristics (Tam 1972, 1991) and resonances (please refer to Edgington-Mitchell (2019) for a recent review).

Coaxial jets have also been a focal point for the scientific community, particularly during the late 1970s when it was discovered that they can exhibit reduced noise levels compared with their equivalent single-jet counterparts under optimal operating conditions (Dosanjh, Abdelhamid & Yu 1969; Dosanjh, Yu & Abdelhailiid 1971; Yu & Dosanjh 1971). Extensive experimental studies have shown that supersonic coaxial jets that operate with a faster external stream, which are known as inverted velocity profile (IVP) jets, can lower the overall jet noise due to a decrease in shock-associated noise. To elucidate this

https://doi.org/10.1017/jfm.2025.156 Published online by Cambridge University Press

phenomenon, a series of experimental and theoretical investigations ensued (Tam & Tanna 1985*a*,*b*; Tanna, Brown & Tam 1985).

In their experimental study, Tanna, Tester & Lau (1979) examined shock-free IVP supersonic jet noise. They observed that IVP jets produce louder high-frequency noise at all angles and quieter low-frequency noise near the jet exit axis. These variations were found to be more pronounced when the velocity ratio of the two streams exceeded 1. The authors concluded that the rapid decay of the maximum mean velocity in IVP jets is a significant factor contributing to the noise reduction in IVP jets compared with single jets. Linear stability studies were subsequently employed to explain the observed trends by Bhat & Seiner (1993) and, later, by Dahl & Morris (1997*a*,*c*,*b*). In particular, the analysis in Dahl & Morris (1997*b*) yielded critical insights into the dynamics of IVP jets. The study focused on the characteristics of the two unstable Kelvin–Helmholtz (K–H) modes supported by the base flow. As expected at supersonic speeds, the first azimuthal Fourier modes ($m = 1$) exhibited higher amplification than their axisymmetric counterparts. The authors showed that, owing to reduced velocity gradients, the instability waves in the inner shear layer were less unstable than those in the outer shear layer. The presence of the inner shear layer was found to affect the dynamics of the outer layer, resulting in higher growth rates and lower phase velocities compared with equivalent single jets. Consequently, the authors theoretically identified that supersonic IVP jets could emit less mixing noise than the reference jet when the velocity ratio is small, the outer stream is hotter than the inner stream and the area ratio is small.

Given the similarities between the nozzle exhaust flow and IVP jets, it is reasonable to expect that the dynamics of nozzle jet flow may resemble that of the IVP jets. However, it is worth noting that, in Dahl & Morris (1997*b*), the study only considered cases where both flow streams were supersonic, while in the nozzle exhaust, the inner flow is decelerated to subsonic speed through a normal shock wave, as depicted in figure 1. In addition, recent studies have highlighted the importance of guided jet modes (GJM) in the dynamics of supersonic jet flows. These waves were first mentioned by Tam & Hu (1989), but were not discussed in Dahl & Morris' paper. In contrast to the K–H waves, these instability waves are neutral duct-like modes (Schmidt *et al.* 2017; Towne *et al.* 2017) that can have the interesting property of propagating in the upstream direction, towards the nozzle. This makes them perfect candidates for providing feedback in a resonance loop (Edgington-Mitchell *et al.* 2018; Gojon, Bogey & Mihaescu 2018; Jaunet *et al.* 2019; Mancinelli *et al.* 2021; Nogueira *et al.* 2022).

To the best of the authors' knowledge, there is no description of such waves in supersonic over-expanded jets, and no model has yet been proposed to predict the occurrence of resonances in the exhaust flow of convergent–divergent nozzles. Therefore, in this study, we investigate the linear dynamics of over-expanded nozzle exhaust flows. A simplified framework of parallel flows is adopted and the study focuses on the effect of the base flow changes, mimicking variations in the nozzle expansion regime, on the characteristics of the most unstable waves and the GJM, which are essential components of some possible feedback resonance process.

2. Dynamical model

2.1. *Base flow modelling*

2.1.1. *Parametrisation of the base flow*

As can be seen in figure 2, the mean flow profiles downstream of the first Mach disk are, as expected, composed of two mixing layers: one separating the supersonic flow

https://doi.org/10.1017/jfm.2025.156 Published online by Cambridge University Press

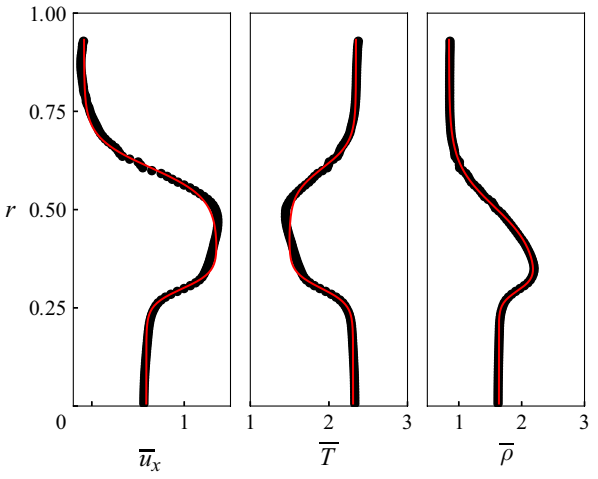


Figure 2. Typical base flow used for the study of local stability properties of the flow. The considered profiles are extracted at the distance from the throat $x/D = 1.6$ (where D is the exit nozzle diameter), in between the two first Mach disks of the flow. Dots represent the numerical data and red lines are the fitted analytical functions.

and the ambient one, the other one separating the subsonic core and the supersonic flow. A representative analytical formulation of this base flow is obtained by connecting three uniform regions, the inner, the annular and the external one, with two hyperbolic tangent profiles to account for the mixing layers:

$$\begin{aligned} q_{in}(r) &= q_i \left[1 - \left(1 - \frac{q_a}{q_i}\right)\left(1 + \tanh\left(\frac{2}{\theta_i}(r - R_i)\right)\right)\right] \\ q_{out}(r) &= 1 - \frac{1}{2}\left(1 - \frac{q_e}{q_a}\right)\left(1 + \tanh\left(\frac{2}{\theta_e}(r - R_e)\right)\right) \\ q(r) &= q_{in}(r) \cdot q_{out}(r), \end{aligned} \tag{2.1}$$

where q here stands for M, $\bar{\rho}$ or $\bar{T}$. The indices i, a, and e respectively refer to the inner, the annular and the external flow variable of interest. The values (R_i, θ_i),(R_e, θ_e) are the inner and external mixing layer radial positions and thicknesses, respectively. A regression of the analytical profiles onto numerical data available (numerical simulation previously done in Bakulu *et al.* (2021)) gives access to the parameters. The reader should note that different mixing layer positions and thicknesses may be attributed to the mean velocity, density or temperature profile when a direct fit to the numerical data are performed. As far as the flow velocity profile is concerned, this formulation is equivalent to the one used in Michalke (1984). This modelisation differs from that chosen by Bhat & Seiner (1993), who preferred Gaussian profiles instead of hyperbolic tangent ones.

Optimal analytical profiles are compared with the reference numerical data in figure 2, demonstrating the ability of the analytical functions chosen to represent the computed flow field. The reader may note that the velocity and temperature profiles are not constant in the supersonic stream. This cannot be accounted for using the chosen analytical formulation and the modelled profiles show a plateau in this region. It is believed that this simplification will not lead to a drastic change in the results, as the velocity and temperature variation within the supersonic stream are very small compared with the variations in the mixing layers.

https://doi.org/10.1017/jfm.2025.156 Published online by Cambridge University Press

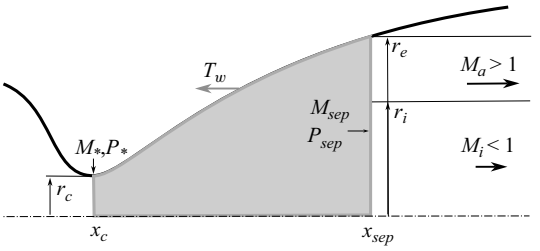


Figure 3. Schematic of the control volume employed to parameterise the flow field.

2.1.2. *Obtaining the base flow parameters*

Annular supersonic flows are commonly encountered when flows exit convergent–divergent nozzles and often exhibit a sufficiently large Mach disk within their core (Hadjadj & Onofri 2009). A simplified analytical description of the shock wave network is proposed in various studies using mass and momentum conservation, for example, in Chow & Chang (1975) and Li & Ben-Dor (1998). We opted to derive an even simpler description of the flow, using quasi-one-dimensional relations, to obtain the parameters that our finite thickness model requires. Indeed, the earlier-presented base flows can be parameterised with the following set of parameters: $(r_i, r_e, M_i, M_e, M_a, T_i, T_a)$. In this section, we often use commas to indicate interchangeable indices for conciseness. For example, the former vector of parameters could be written as $(r_{i,e}, M_{i,e,a}, T_{i,a})$ with this notation. Basic fluid mechanics principles reveal that these parameters are interconnected and we cannot assume arbitrary values. Hence, to attain a meaningful parameter set, a simplified model of the flow inside the nozzle is built, assuming quasi-one-dimensional behaviour from the throat to the separation point, where the annular supersonic flow is presumed to originate. The simplified flow configuration and the associated control volume that we use for that purpose are illustrated in figure 3.

By applying mass conservation to the control volume bounded by the nozzle throat and the attached flow (as depicted in grey in figure 3), we derive the equation

$$\rho_* U_* D_c^2 = \rho_i U_i D_i^2 + \rho_a U_a (1 - D_i^2), \tag{2.2}$$

where $(\cdot)_*$ denotes sonic variables at the throat and $D_{i,c} = D_{i,c}/D_e$ represents the normalised radius of the inner $(\cdot_i)$ vortex sheet or the throat $(\cdot_c)$ relative to the external vortex sheet.

Noting that $\mathcal{M}$, the local Mach number, differs from the acoustic Mach number employed in the subsequent linearised dynamical model, $\mathcal{M} = M \cdot c_\infty/c$, where c is the local speed of sound, the following relation can be easily obtained from the previous equation:

$$\left(1 + \frac{\gamma - 1}{2}\right)^{-\frac{\gamma+1}{2(\gamma-1)}} \frac{P_{t0}}{\sqrt{T_{t0}}} D_c^2 = \frac{P_i}{\sqrt{T_i}} \mathcal{M}_i D_i^2 + \frac{P_a}{\sqrt{T_a}} \mathcal{M}_a (1 - D_i^2), \tag{2.3}$$

where P_{t0} and T_{t0}, respectively, are the total pressure and temperature of the flow, and $P_{i,a}$ and $T_{i,a}$, respectively, are the static pressure and temperature of the inner $(\cdot, i)$ and annular $(\cdot, a)$ streams. Assuming an isobaric jet for simplification, i.e. $P_a = P_i = P_\infty$, the mass conservation equation can be further simplified to (see Appendix A for further details)

$$\beta_m D_c^2 = (\mu_i - \mu_a) D_i^2 + \mu_a, \tag{2.4}$$

https://doi.org/10.1017/jfm.2025.156 Published online by Cambridge University Press

where

$$\mu_{i,a} = \mathcal{M}_{i,a}\sqrt{1+\frac{\gamma-1}{2}\mathcal{M}_{i,a}^2} \tag{2.5}$$

$$\beta_m = \left(1+\frac{\gamma-1}{2}\right)^{-\frac{\gamma+1}{2(\gamma-1)}}\frac{P_{t0}}{P_\infty}. \tag{2.6}$$

In essence, the mass conservation equation establishes a connection between the nozzle pressure ratio $NPR = P_{t0}/P_\infty$, its geometry and the Mach numbers of both the annular and internal jets. The NPR is dictated by the nozzle's operational regime, and D_c is given by nozzle design considerations.

Considering momentum conservation along the axial direction within the same control volume, while neglecting body and viscous forces, leads to the equation

$$\beta_q D_c^2 - \frac{F_w}{P_\infty} = \gamma D_i^2\left(\mathcal{M}_i^2 - \mathcal{M}_a^2\right) + \left(\gamma\mathcal{M}_a^2+1\right), \tag{2.7}$$

where

$$\beta_q = (1+\gamma)\left(1+\frac{\gamma-1}{2}\right)^{\frac{-\gamma}{\gamma-1}}\frac{P_{t0}}{P_\infty}, \tag{2.8}$$

and F_w represents the pressure forces acting on the nozzle wall. It is important to note that F_w depends on the nozzle geometry and can be approximated using characteristic methods. By solving this equation, we derive an analytical expression for D_i^2 given by

$$D_i^2 = \frac{1}{\gamma\left(\mathcal{M}_i^2 - \mathcal{M}_a^2\right)}\left[\beta_q D_c^2 - \frac{F_w}{P_\infty} - \left(\gamma\mathcal{M}_a^2+1\right)\right], \tag{2.9}$$

which can subsequently be substituted into the mass conservation equation. This substitution leads to an equation for the annular Mach number, providing that $\mathcal{M}_i$ and F_w are known:

$$\frac{\mu_i - \mu_a}{\gamma\left(\mathcal{M}_i^2 - \mathcal{M}_a^2\right)}\left[\beta_q D_c^2 - \frac{F_w}{P_\infty} - \left(\gamma\mathcal{M}_a^2+1\right)\right] + \mu_a - \beta_m = 0, \tag{2.10}$$

where

$$\mu_{i,a} = \mathcal{M}_{i,a}\sqrt{1+\frac{\gamma-1}{2}\mathcal{M}_{i,a}^2} \tag{2.11}$$

$$\beta_m = \left(1+\frac{\gamma-1}{2}\right)^{-\frac{\gamma+1}{2(\gamma-1)}}\frac{P_{t0}}{P_\infty} \tag{2.12}$$

$$\beta_q = (1+\gamma)\left(1+\frac{\gamma-1}{2}\right)^{\frac{-\gamma}{\gamma-1}}\frac{P_{t0}}{P_\infty}. \tag{2.13}$$

It is worth mentioning that, once $M_{i,a}$ are known, $T_{i,a}$ can be determined via the usual isentropic relations, using the typically known total temperature of the flow.

2.1.3. *Solving the base flow model*

Equation (2.10) can be solved to determine the Mach number of the annular flow, adhering to the fundamental principles of fluid mechanics. This can be achieved for any given input parameter set containing the nozzle pressure ratio $NPR = P_{t0}/P_\infty$, throat diameter D_c,

https://doi.org/10.1017/jfm.2025.156 Published online by Cambridge University Press

inner subsonic Mach number $\mathcal{M}_i$ and nozzle thrust F_w. These parameters are intrinsically interconnected and must be chosen judiciously. In what follows, we elucidate how these parameters can be defined based on the nozzle's pressure and Mach number profiles, along with the application of a classical separation criterion. We assume that flow separation occurs at an axial location within the nozzle, denoted by x_{sep}, where an isentropic expansion of the flow inside the nozzle has resulted in a local Mach number $\mathcal{M}_{sep}$ and pressure P_{sep}.

First, it is evident from figure 3 that our reference length scale, D_e, can be equated to the diameter of the nozzle at the separation point D_w:

$$D_e = D_w(x_{sep}). \tag{2.14}$$

This implies that the reference length scale for the annular jet flow will vary according to the NPR.

Second, experimental observations suggest that the separation pressure P_{sep} is related to the separation Mach number and the external pressure P_∞ through a suitably chosen separation criterion:

$$\frac{P_{sep}}{P_\infty} = F(\mathcal{M}_{sep}), \tag{2.15}$$

where F represents the separation criterion formula, which enables the determination of P_{sep}. Subsequently, assuming an isentropic expansion from the tank to the separation point, the NPR at the current flow condition can be calculated as

$$\frac{P_{t0}}{P_\infty} = F(\mathcal{M}_{sep})\left(1 + \frac{\gamma - 1}{2}\mathcal{M}_{sep}\right)^{\frac{\gamma}{\gamma-1}}. \tag{2.16}$$

An approximation for the inner Mach number $\mathcal{M}_i$ can be derived by considering that the Mach disk is formed at the upstream Mach number $\mathcal{M}_{sep}$:

$$\mathcal{M}_i = \frac{(\gamma - 1)\mathcal{M}_{sep}^2 + 2}{2\gamma\mathcal{M}_{sep}^2 - (\gamma - 1)}. \tag{2.17}$$

It is important to note that this approximation leads to an overestimation of $\mathcal{M}_i$ since, in real flow conditions, the Mach disk always forms downstream of the separation point, and hence at higher Mach numbers.

Finally, the thrust of the control volume, F_w, can be determined by integrating the wall pressure along the nozzle from the throat to the separation point x_{sep}:

$$F_w = \int_{x_c}^{x_{sep}} (P_\infty - P_w)\,(\boldsymbol{n}\cdot\boldsymbol{i})\,\mathrm{d}S. \tag{2.18}$$

The model is now complete and only requires the nozzle wall radius and Mach number profiles, which can be computed using methods such as the method of characteristics. An example using nozzle characteristics from Jaunet *et al.* (2017) is presented in the following section. The acoustic Mach numbers of the vortex sheets and the inner radius satisfying the proposed model are depicted in figure 4 against the fully expanded Mach number of the flow M_j. The value of M_j can be computed easily from the nozzle NPR using isentropic relations. The separation criterion from Stark (2005), with slight modifications to better align with the experimental observations of Jaunet *et al.* (2017) for this nozzle geometry, is employed. The decrease in $\mathcal{M}_i$ as the normal shock wave strengthens with downstream displacement of the separation, is in accordance with expectations. Conversely, neither M_a nor D_i display a monotonic behaviour. This can be attributed to the nozzle wall

https://doi.org/10.1017/jfm.2025.156 Published online by Cambridge University Press

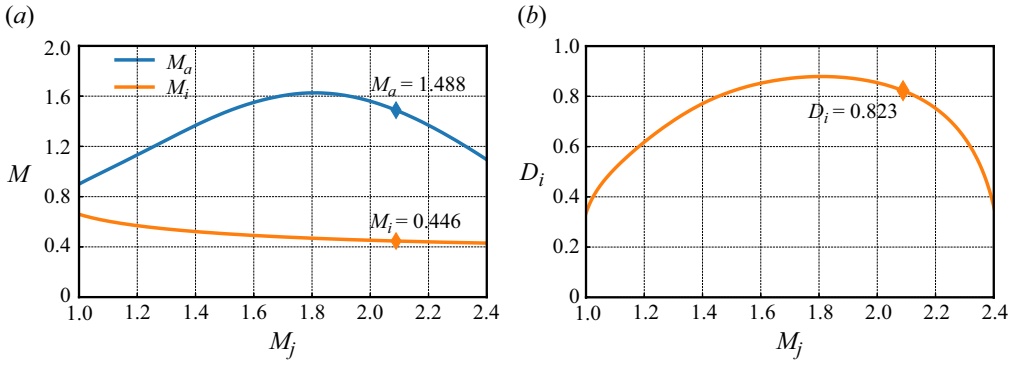


Figure 4. Variation of Mach numbers (*a*) and location of inner vortex sheet diameters (*b*) with the fully expanded jet Mach number.

	M_i	M_a	D_i
DDES	0.40	1.42	0.48
Model	0.446	1.488	0.82

Table 1. Comparison of Mach numbers and inner shear layer locations obtained from the DDES of Bakulu *et al.* (2021) and the proposed simplified model.

profile approaching a near-horizontal orientation near the lip, resulting in saturation of thrust F_w. Another noteworthy behaviour is the sudden decrease in D_i as the separation approaches the nozzle lip, which is consistent with the behaviour of overexpanded jets from TIC nozzles – akin to an approaching adaptation where the Mach disk diminishes or disappears.

Mach number and inner shear layer location values obtained for $M_j = 2.09$ are indicated as diamonds in figure 4. Table 1 compares the predictions of the model with those observed in numerical simulations from Bakulu *et al.* (2021), specifically after the first Mach disk. The results are summarised in table 1. As seen, the proposed model accurately predicts Mach numbers within a $\pm 10\,\%$ range but tends to overestimate D_i. This discrepancy is due to assuming a horizontal flow exit from separation, which is erroneous as the flow is deflected through the separation shock wave. However, this representation acknowledges its simplified nature. Adjusting the empirical separation model, or using a more representative value for D_e, would yield slightly different values for $M_{i,a}$ and D_i. Despite these uncertainties, it is believed that the model remains valuable for understanding the overall dynamics of the flow.

In conclusion, we have formulated a comprehensive model that derives essential parameters for feeding a simplified linear dynamical model of jet flows exiting from over-expanded nozzles. This model requires the *a priori* knowledge of the static pressure and Mach number profiles along the nozzle, and a separation criterion. From this, all the necessary quantities to build a simplified mean annular supersonic mean flow for various nozzle regimes can be retrieved.

2.2. *Finite thickness dynamical model*

We use the same approach as Mancinelli *et al.* (2021), modelling the jet using locally parallel linear stability theory. All variables are normalised by the fully expanded jet

https://doi.org/10.1017/jfm.2025.156 Published online by Cambridge University Press

diameter D_j, the ambient density and the speed of sound ρ_∞ and c_∞, respectively. The Reynolds decomposition,

$$\boldsymbol{q}(x, r, \theta, t) = \overline{\boldsymbol{q}}(r) + \boldsymbol{q}'(x, r, \theta, t), \tag{2.19}$$

is applied to the flow-state vector $\boldsymbol{q}$, where the mean and fluctuating components are $\overline{\boldsymbol{q}}$ and $\boldsymbol{q}'$, respectively. We assume the normal-mode ansatz,

$$\boldsymbol{q}(x, r, \theta, t) = \hat{\boldsymbol{q}}(r)\mathrm{e}^{\mathrm{i}(kx+m\theta-\omega t)} \tag{2.20}$$

where k is the streamwise wavenumber and m is the azimuthal Fourier wavenumber. The non-dimensional pulsation $\omega = 2\pi St M_a$ is computed via the acoustic Mach number of the jet $M_a = U_j/c_\infty$ and the Strouhal number of the flow $St = fD_j/U_j$, where U_j and D_j are the equivalent fully expanded velocity of the flow and diameter of the jet, respectively.

Linearising the Euler equation around the base flow, we obtain the compressible Rayleigh equation for pressure,

$$\frac{\partial^2 \hat{p}}{\partial r^2} + \left(\frac{1}{r} - \frac{2k}{\overline{u}_x k - \omega}\frac{\partial \overline{u}_x}{\partial r} - \frac{\gamma - 1}{\gamma \overline{\rho}}\frac{\partial \overline{\rho}}{\partial r} + \frac{1}{\gamma \overline{T}}\frac{\partial \overline{T}}{\partial r}\right)\frac{\partial \hat{p}}{\partial r} - \left(k^2 + \frac{m^2}{r^2} - \frac{(\overline{u}_x k - \omega)^2}{(\gamma - 1)\overline{T}}\right)\hat{p} = 0, \tag{2.21}$$

where γ is the specific heat ratio for a perfect gas. The solution of the linear stability problem is obtained by specifying a real or complex frequency ω and solving the resulting augmented eigenvalue problem $k = k(\omega)$, with $\hat{p}(r)$ being the associated pressure eigenfunction. The eigenvalue problem is solved numerically by discretising (2.21) in the radial direction using Chebyshev polynomials. A mapping function is used to non-uniformly distribute the grid points such that they are dense in the region of shear (Trefethen 2000).

Although the model we have described supports the non-isobaric regime (Mancinelli *et al.* 2023), only isobaric and isothermal jets will be studied in the following. Moreover, only the first non-axisymmetric fluctuating mode ($m = 1$) is considered, because this azimuthal mode is the only one responsible for side-loads in overexpanded nozzle flows (Dumnov 1996) and for resonances observed in experiments (Jaunet *et al.* 2017).

The flow dynamics is also studied without taking the nozzle walls into account. This corresponds to a free-jet configuration and we are looking for pressure waves vanishing at infinity. This choice is motivated by the fact that, in our previous observations, the downstream- and uptream-propagating wave signatures were observed as being dominant far downstream of the nozzle, where the influence of the nozzle wall is negligible.

2.3. *Convergence of the linear stability calculation*

In figure 5, we present the convergence of the eigenvalue spectrum with respect to the number of Chebychev collocation points N and the Strouhal number. We indicate in figure 5 the position of the waves of interest in this paper, namely, the GJM and the two unstable waves ($k_i < 0$) that lie in the $k_r > 0$ portion of the spectrum and are travelling downstream. These modes will be named inner and outer K–H waves in this article as they have spatial support with a maximum located on both the inner and the outer mixing layers, as expected for K–H waves. This denomination seems logical, although it will be shown later that their spatial supports show some differences, in particular, regarding their decay in the radial direction. This might need a separate discussion in itself, but it is out of the scope of the curent study.

https://doi.org/10.1017/jfm.2025.156 Published online by Cambridge University Press

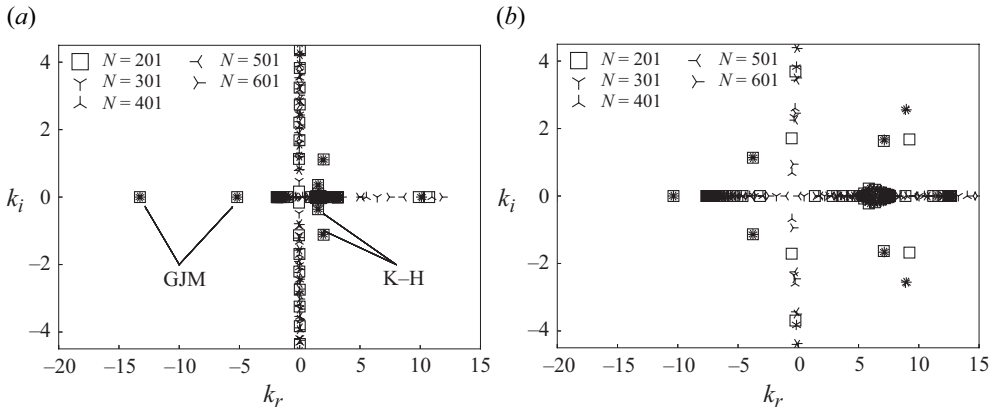


Figure 5. Convergence of the eigenvalue spectrum with respect to the number of Chebychev collocation points for $St = 0.1$ (*a*) and $St = 0.4$ (*b*).

The GJM, on the other hand, lie in the $k_r < 0$ region and on the real axis, and hence they are neutral waves with negative phase speed. The positions of these modes change with varying frequency. The GJM moves along the real axis and might separate from this axis and become evanescent. This is what is shown in figure 5 right, where two GJM can be seen near the $(-5, \pm 1.5)$ position. For a more precise discussion on these modes, we refer the reader to Towne *et al.* (2017).

The overlay of the different symbols in figure 5 shows that the convergence is more difficult to reach at high frequencies, especially for the K–H modes, but the spectrum seems to have converged for more than $N = 301$ points for the frequencies of interest in this paper. Therefore, a total number of $N = 401$ collocation points is used for all the computations in this study.

3. Dynamics of annular supersonic jets

In contrast to a single-stream jet flow, the base flow of a annular jet requires more parameters to be perfectly described. The characteristic features of the base flow (mixing layer thickness or position) may also evolve with the nozzle pressure ratio; therefore, its relative influence on the stability spectrum needs to be evaluated before one may explore the conditions for resonance. For this purpose, we use the analytical profile described previously and explore the influence of the main parameters on the stability properties of the jet.

3.1. *Effect of radial position*

The influence of the relative positions of the mixing layers was first studied by assuming a constant reference velocity level in the subsonic core and the supersonic stream. We performed linear stability analyses by varying the position of the inner mixing layer and keeping that of the outer mixing layer constant, as presented in figure 6. The inner, annular and external Mach numbers were chosen to approximately match the numerical simulations downstream of the first Mach disk: i.e. $M_i = 0.6$, $M_a = 1.4$ and $M_e = 0$. The density profile was computed using the Crocco–Busemann relation (Michalke 1984). A total of 36 base flows was used to finely study the changes in the corresponding linear dynamics.

https://doi.org/10.1017/jfm.2025.156 Published online by Cambridge University Press

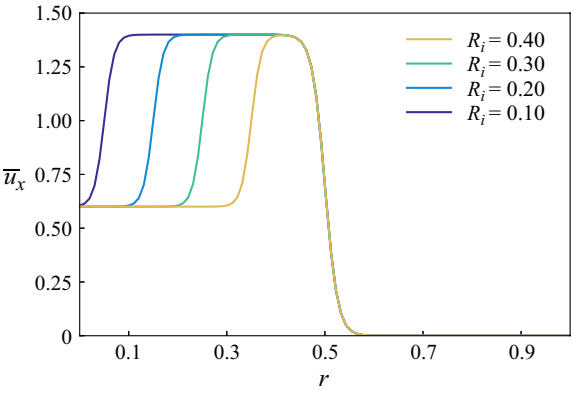


Figure 6. Base flows used to study the effect of the position of the inner mixing layer on the flow dynamics.

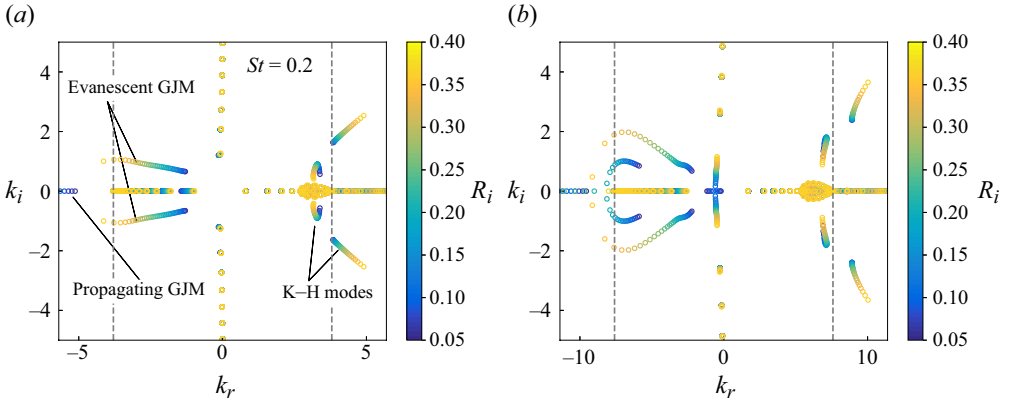


Figure 7. Eigenspectra computed at $St = 0.2$ and $St = 0.4$ for various R_i. The dashed lines indicate the wavenumber corresponding to sonic phase speed.

Typical eigenspectra obtained at $St = 0.2$ and $m = 1$ are presented in figure 7. On the right-hand side of the figure ($k_r > 0$), two groups of unstable eigenvalues (i.e. belonging to the $k_i < 0$ half-plane) can be observed. They correspond to the K–H modes of both the inner and outer mixing layers, as was found by Dahl & Morris (1997*b*) for supersonic IVP jets. The inner K–H mode is the least unstable of the two. The vertical ($k_r = 0$) and horizontal ($k_i = 0$) parts of the continuous acoustic branch are clearly visible, with a relatively weak influence of R_i on the loci of the corresponding eigenvalues. Propagating and evanescent GJM (Towne *et al.* 2017) can also be identified in the $k_r < 0$ half-plane. Thus, the annular supersonic jets appear to exhibit similar features to those of a classical top-hat supersonic jet. In the following, we focus on extracting the effect of the inner mixing layer position on the characteristics of these waves.

3.1.1. *K–H mode*

In figure 8, we plot the growth rate evolution of both K–H modes as a function of R_i for various Strouhal numbers. The outer K–H mode is always more unstable than the inner one for all the configurations investigated in this study. This is expected considering that the velocity gradient is stronger for the outer mixing layer than for the inner one. The outer mode becomes even more unstable as R_i increases, although at high frequencies its

https://doi.org/10.1017/jfm.2025.156 Published online by Cambridge University Press

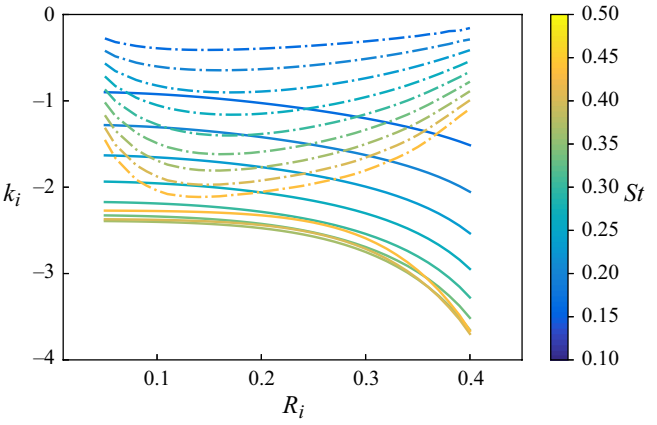


Figure 8. Growth rate of the K–H mode as a function of the Strouhal number and the inner mixing layer location R_i. Dashed lines and solid lines correspond to the inner and outer K–H modes, respectively.

growth rate shows a plateau at low values of R_i. On the other hand, the inner mixing layer instability shows an optimal growth rate at specific R_i values. This trend suggests that there may exist specific base flows and frequencies for which the inner and outer K–H modes possess equivalent growth rates. In some cases, the inner mode can become even more unstable than the outer one. However, this is more likely to occur at higher frequencies and might not be relevant for the initial nozzle flow problem, where resonance at lower frequencies is observed.

The pressure eigenfunctions associated with the two identified K–H modes are presented in figure 9 for $St = 0.2$. As expected, the eigenfunction is maximum at the mixing layer location and is zero at the centre line, as we focus on the $m = 1$ anti-symmetric wavenumber. The outer K–H mode does not seem to be significantly affected by the inner mixing layer, unlike the inner mode whose support spreads further to the outside the outer mixing layer as the two mixing layers get closer. Interestingly, the radial support of the inner K–H wave decays less rapidly than that of the outer one. This allows the inner mode to be detected quite far from the jet and enables it to exchange energy with feedback waves outside the supersonic annular region. This aligns well with the observations of Bakulu *et al.* (2021), who found that the inner mixing layer supports most of the perturbations associated with the resonance process in their flow.

3.1.2. *GJM*

GJM have been shown to play a significant role in the resonance of screeching and impinging jets (see, for example, Gojon *et al.* (2018); Jaunet *et al.* (2019); Mancinelli *et al.* (2021); Edgington-Mitchell *et al.* (2018)). Their dispersion relation is a key characteristic that explains cut-on and cut-off frequencies, and the transition from axisymmetric to helical modes, and it improves the model predictions (Mancinelli *et al.* 2019; Nogueira *et al.* 2022). As explained previously, their eigenvalues lie on the real axis of the spectrum until they become evanescent. Figure 7 shows that the annular jet configuration, as encountered in the exhaust of over-expanded Convergent-Divergent (CD) nozzles, also supports such types of waves. In the (k_r, St) plane, this occurs at the summit of a given branch. At supersonic speeds, jets support both upstream propagation, denoted by k_p^-, and downstream propagation, denoted by k_p^+, GJM. This distinction is made based on the sign of their group velocity $u_g = \partial\omega/\partial k$, and hence corresponds to the local slope of their dispersion relation presented in figure 10. The k_p^- can be seen close to the acoustic waves

https://doi.org/10.1017/jfm.2025.156 Published online by Cambridge University Press

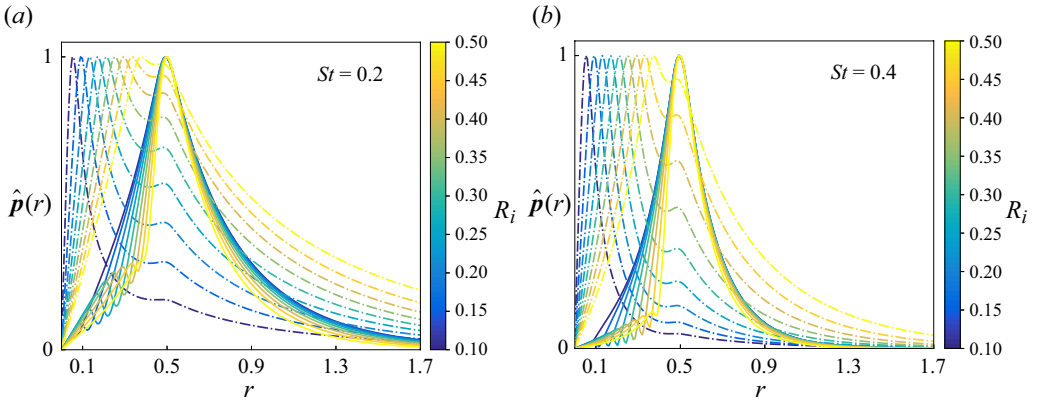


Figure 9. Eigenfunctions associated with the inner (dashed) and outer (solid) K–H modes, normalised with respect to their maximum values, for $St = 0.2$ and $St = 0.4$.

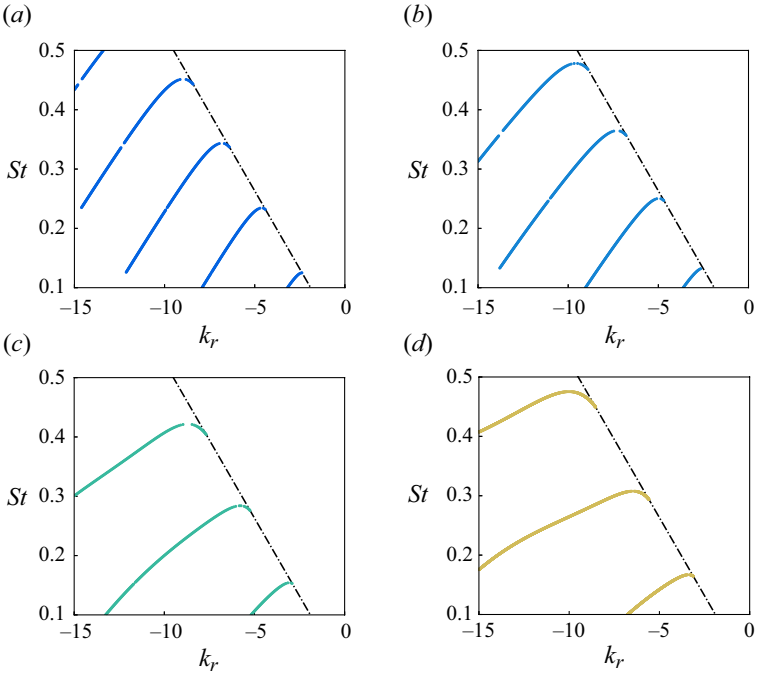


Figure 10. Neutral mode dispersion relation for various positions of the inner mixing layer: $R_i = 0.05$ (a),$R_i = 0.1$ (b),$R_i = 0.2$ (c) and $R_i = 0.30$ (d). The dash-dotted line corresponds to the acoustic wave dispersion relation.

dispersion relation and is the mode that can carry energy in the upstream direction. The dispersion relation of these waves is plotted in figure 10 in the $St-k_r$ plane for various positions of the inner mixing layer.

As expected, at each R_i, the neutral waves form families of modes hierarchically ordered by their radial supports: higher frequencies correspond to higher radial orders (i.e. the number of nodes and antinodes; see Tam & Hu (1989)). As seen, the position of the inner mixing layer has a strong impact on the dispersion relation of the neutral modes: as R_i increases, the frequencies at which the modes are encountered also increase. Furthermore,

https://doi.org/10.1017/jfm.2025.156 Published online by Cambridge University Press

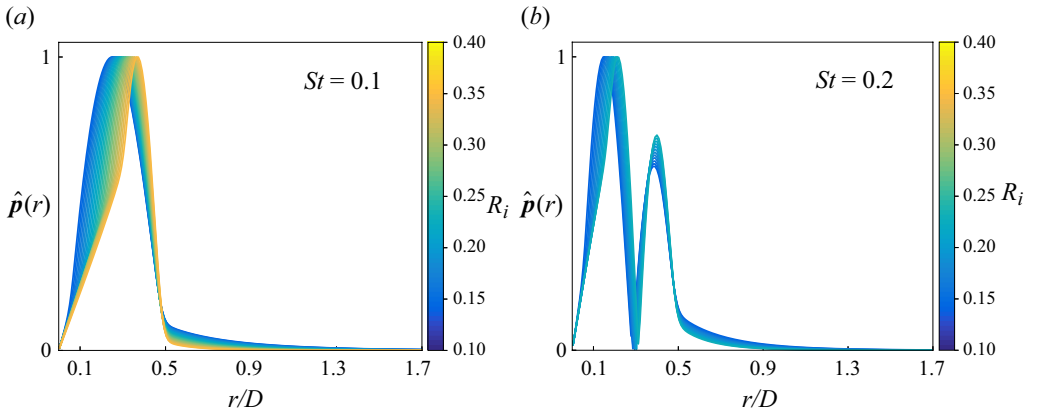


Figure 11. Eigenfunctions associated with the guided jet modes, normalised with respect to their maximum values, for $St = 0.1$ and $St = 0.2$.

the group velocity of the k_p^+ mode decreases with increasing R_i. This can be understood by recognising that, for $R_i = 0$ or $R_i = R_e$, the base flow is close to a supersonic top-hat jet or a subsonic one, respectively. As can be seen, both group and phase velocities of the guided jet modes decrease with increasing R_i. This is expected from the decrease of the overall average speed of the jet when R_i increases. The behaviour of the neutral modes seems to lie between what is expected for a subsonic $M = M_i < 1.0$ jet and a supersonic $M = M_a > 1.0$ one.

Moreover, we observe that R_i affects the domain of existence of the upstream propagating neutral modes, which are the modes in the dispersion relation with negative group velocity. First, the domain where $d\omega/dk < 0$ shifts towards higher Strouhal numbers with increasing R_i. Second, the range of Strouhal numbers where these neutral modes are encountered varies significantly with R_i: larger R_i providing a wider range of existence, and therefore offering more solutions for possible resonances.

The eigenfunctions associated with the upstream propagating neutral modes are presented in figure 11 for $St = 0.1$ and $St = 0.2$. As expected, the radial supports of these modes share common features with Bessel functions. At low Strouhal numbers, the eigenfunctions show one antinode, while for higher frequencies, more antinodes can be observed. Surprisingly, very little change in the radial support is observed for varying R_i. This is due to the fact that these modes are duct-like modes, so that their support is mostly independent of the base flow, in contrast to their wavenumber. It is important to notice that they also have support outside the jet, similar to the inner K–H wave. This allows these waves to interact and for the upstream mode to carry energy upstream, potentially closing a feedback loop.

3.2. *Effect of mixing layer thickness*

To explore the influence of the thicknesses of the mixing layers on the stability properties of the flow, we varied the base flow as presented in figure 12. Both mixing layers are centred around $D_j/2$ and $D_j/4$. The jet bulk velocities were chosen to be constant and comparable with those observed in the nozzle after the first Mach disk for the case previously studied at $M_j = 2.1$.

https://doi.org/10.1017/jfm.2025.156 Published online by Cambridge University Press

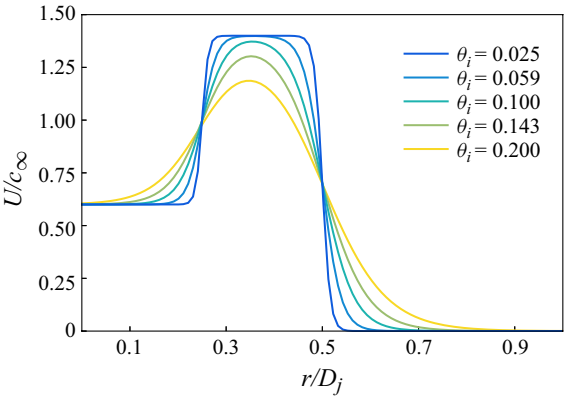


Figure 12. Base flows used to study the effect of mixing layer thickness.

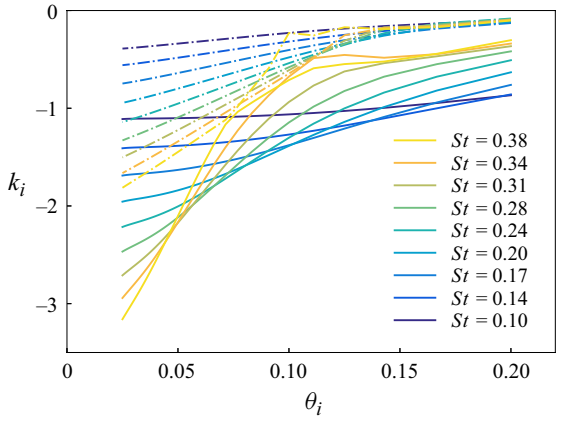


Figure 13. Growth rates of both the inner (_ _ _) and outer (____) K–H modes as functions of the mixing layer thicknesses and the Strouhal number.

3.2.1. *K–H mode*

Figure 13 shows the growth rate of both K–H modes with varying thicknesses and Strouhal numbers. As expected, larger mixing layer thicknesses result in lower growth rates of the K–H mode. For the base flows and frequencies considered here, the inner mixing layer is more stable than the outer one. This is due to their difference in velocity gradient. The outer mixing layer separates a supersonic stream from a quiescent atmosphere, while the inner one separates two rapid flows. Interestingly, for relatively high frequencies (greater than $St = 0.2$), increasing the thickness stabilises the outer mixing layer more quickly than the inner one. Thus, there might be flow configurations for which both K–H modes exhibit comparable growth rates. Depending on the frequency and base flow, the dynamics may not be entirely dominated by the outer K–H mode, as one might initially assume.

The associated spatial profiles of the aforementioned K–H modes are presented in figure 14 for different Strouhal numbers and varying mixing layer thicknesses. We observe similar results to the previous study: for the thinnest mixing layer, the inner and outer K–H modes exhibit maximum pressure fluctuations at the locations where the base flow exhibits the maximum levels of velocity gradients. For all frequencies, thickening the mixing layer tends to spread the spatial support of the inner modes towards the outer mixing layer by

https://doi.org/10.1017/jfm.2025.156 Published online by Cambridge University Press

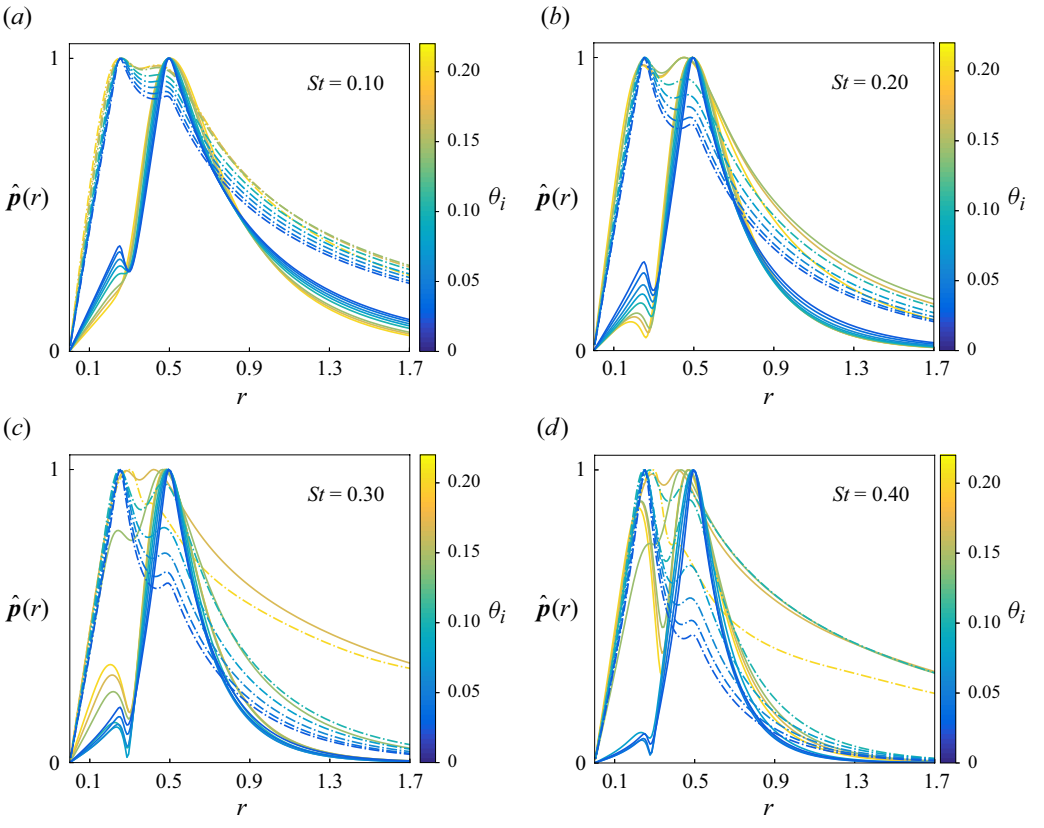


Figure 14. Eigenfunctions associated with the inner (dashed) and outer (plain) K–H modes, normalised with respect to their maximum values, for $St = 0.1$ (*a*), $St = 0.2$ (*b*), $St = 0.3$ (*c*) and $St = 0.4$ (*d*).

increasing the pressure amplitude near the jet boundary. At the highest frequencies studied here, the signature of the outer K–H modes also spreads onto the inner mixing layer. As indicated earlier by their relative growth rates, the entanglement of spatial support of the K–H modes with increasing mixing layer thickness might make it difficult to distinguish their relative signatures in the fluctuating pressure field. Nonetheless, as mentioned in the previous section, the inner mixing layer K–H mode appears to have a slower radial decay compared with the outer one. This supports the findings of Bakulu *et al.* (2021), which show that, at the resonance frequency, the downstream energy-carrying mode was supported by the inner mixing layer. The wide radial extent of the eigenfunction, as shown here, also suggests that the inner K–H mode can exchange energy with GJM or acoustic modes, whose support can be located outside the jet.

3.2.2. *GJM*

The dispersion relation of the GJM for varying mixing layer thicknesses is now presented in figure 15. Unlike the dispersion relation of K–H modes, the dispersion relation of the GJM is only slightly affected by thicknesses of the mixing layers. There is a slight variation in the domain of existence of the upstream-travelling modes between the branch and saddle points, as pointed out by Towne *et al.* (2017). The primary effect of thickening the mixing layers is on the group velocity ($\partial\omega/\partial k$), with thicker mixing layers leading to lower group velocities, as one would expect.

https://doi.org/10.1017/jfm.2025.156 Published online by Cambridge University Press

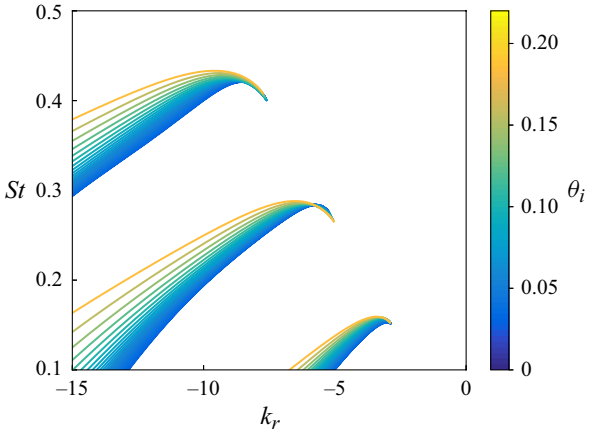


Figure 15. GJM dispersion relationship for varying mixing layer thicknesses.

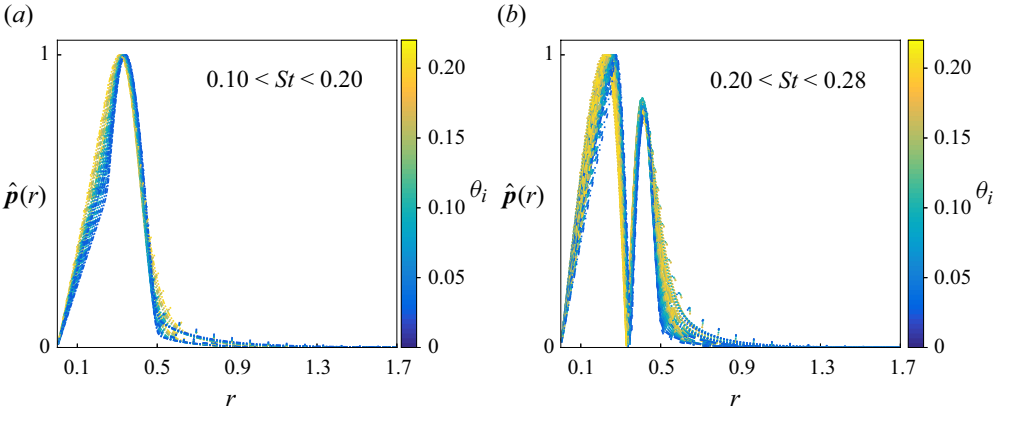


Figure 16. GJM spatial support for the first radial order (*a*) and the second radial order (*b*). Colors indicate the mixing layer vorticity thickness, and different line styles are attributed to eigenfunctions of different frequencies.

Figure 16 presents the eigenfunctions of the computed GJM. Frequencies were selected so that modes of the same radial order appear on the same figure. Note that eigenfunctions obtained at the same frequency are plotted with the same line style. All computed eigenfunctions almost collapse onto the same line, indicating that the spatial support of the GJM is not affected by the thickening of the jet. The GJM are very robust and can still be observed even if the jet is strongly affected by the diffusion of momentum across the stream interfaces.

3.3. *Stability properties of the flow with varying NPR*

Using the simple base flow model described in § 2.1.2, we obtained all the necessary parameters to build simplified base flows for M_j varying between 1.7 and 2.2, corresponding to expansion regimes where resonances were observed for the TIC nozzle geometry previously studied (Jaunet *et al.* 2017). The aforementioned base flows are presented in figure 17, where the reader can see that the position of the inner mixing layer, as well as both the inner and annular flow velocity, vary with the chosen jet Mach number, their trends being in agreement with the results of figure 4. Regarding the thickness of the

https://doi.org/10.1017/jfm.2025.156 Published online by Cambridge University Press

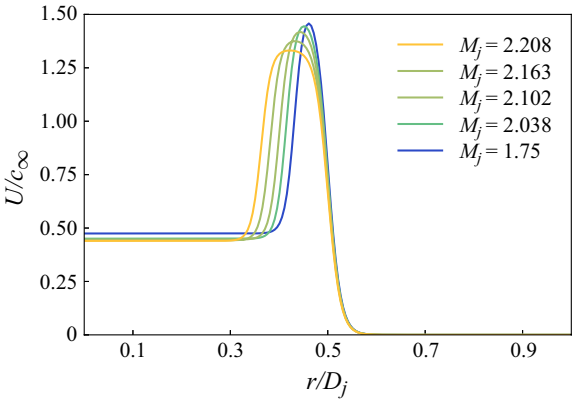


Figure 17. Base flows used to study the effect of the expansion regime on the stability characteristics of the flow.

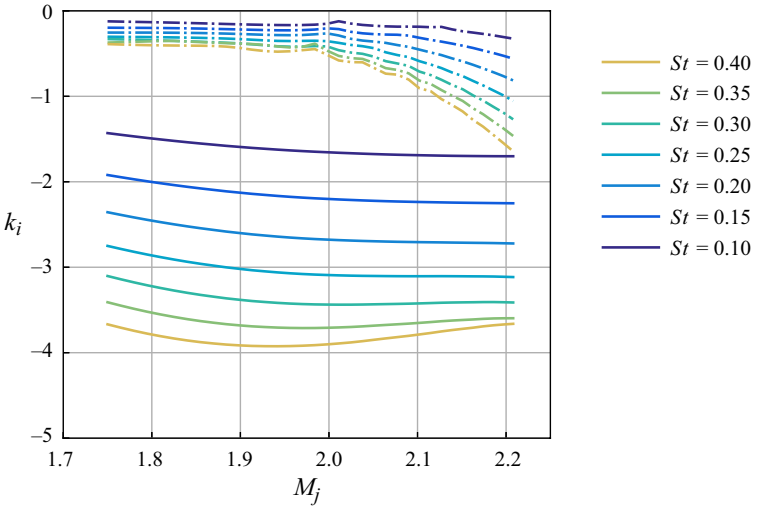


Figure 18. Growth rate of both the innner (- - -) and outer (——) K–H modes for varying jet Mach number M_j and Strouhal number.

mixing layers, we used that obtained from the numerical results shown in figure 2 for all cases. In spite of this simplification, it is believed that, given the relative narrow range of jet Mach number considered, the exact mixing layer shape may not drastically change.

3.3.1. *K–H modes*

The dynamical characteristics of the unstable K–H waves with respect to the base flows presented in the former paragraph are plotted in figure 18 for various frequencies. As expected from the previous results, both K–H waves are unstable, the outer one being the most unstable for all flow regimes and frequencies considered. The evolution of the growth rate of the inner K–H wave seems rather independent of the jet Mach number until $M_j = 2.0$. For values greater than this expansion ratio, it is interesting to notice that the inner K–H wave is more and more unstable at all the frequencies considered. It is worth noting that this value is very close to the value of $M_j = 2.09$ around which resonances have been experimentally observed (Jaunet *et al.* 2017). The close agreement of these experimental

https://doi.org/10.1017/jfm.2025.156 Published online by Cambridge University Press

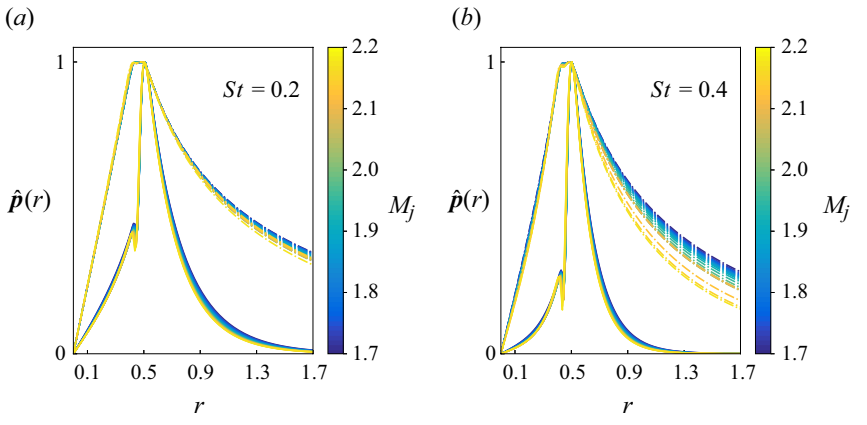


Figure 19. Eigenfunction of both the innner (- - -) and outer (——) K–H modes for varying jet Mach number Mj and Strouhal number.

and theoretical values is very striking and still supports the idea that resonance in TIC nozzles may only be allowed when the inner mixing layer becomes sufficiently unstable.

In figure 19, we show the pressure eigenfunctions of both K–H modes. The outer K–H is well localised at the location of maximum shear in the outer mixing layer and decays exponentially in the radial direction. For all the cases considered here, the inner K–H mode spatial support is more widely spread across the jet and shows a slower radial decay that the outer one. Overall, the K–H waves computed in those cases show the same characteristics as previously reported. The reader should notice, however, that the spatial support of the K–H waves computed does not depend on the Strouhal number nor the jet Mach number.

3.3.2. *GJM*

As far as GJM are concerned, the expansion ratio of the nozzle plays a significant role in their dispersion relation, as can be seen in figure 20. At low M_j, the slope of the dispersion relation is negative and does not show any extrema; hence, only upstream propagating GJM seem supported by the flow field. As depicted earlier in the study, this is an effect of the thinning of the annular jet that provides the modes with a behaviour encountered in subsonic jet (Towne *et al.* 2017; Jordan *et al.* 2018). As soon as the overall speed of the jet increases, the GJM dispersion relation deforms towards what is expected in supersonic cases, where the dispersion relation is constituted by both downstream- ($(\partial\omega/\partial k) > 0$) and upstream-propagating ($(\partial\omega/\partial k) < 0$) branches. In any case, the results show that, for all expansion ratios, the flow supports an upstream-propagating wave that makes resonance loops possible.

3.3.3. *Discussion*

According to figure 20, the dynamical model does not show any upstream propagating waves for $M_j = 2.09$ at $St = 0.2$, although a resonance was experimentally and numerically observed (Jaunet *et al.* 2017; Bakulu *et al.* 2021). This means that it would not be possible with the current base flow and finite thickness models to predict a resonance at the correct Mach and Strouhal numbers in over-expanded flows, with a similar mechanism as depicted for screech-like resonance. This is mainly due to the numerous hypotheses and simplifications that are embedded in these models.

The sensitivity of the dispersion relation of the waves and the stability characteristics to the base flow, shown in the previous section, indicate that a more precise definition of

https://doi.org/10.1017/jfm.2025.156 Published online by Cambridge University Press

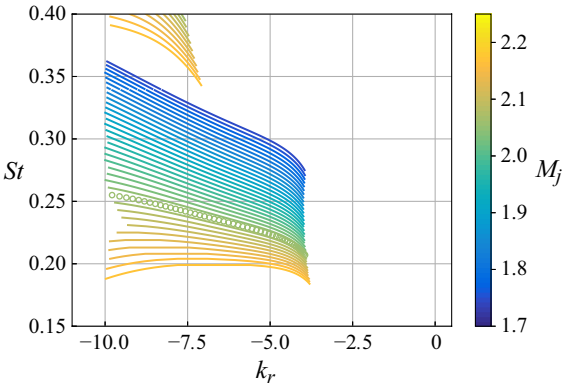


Figure 20. Dispersion relation of the GJM for varying nozzle expansion ratios. The circles represents the dispertion relation for $M_j = 2.09$.

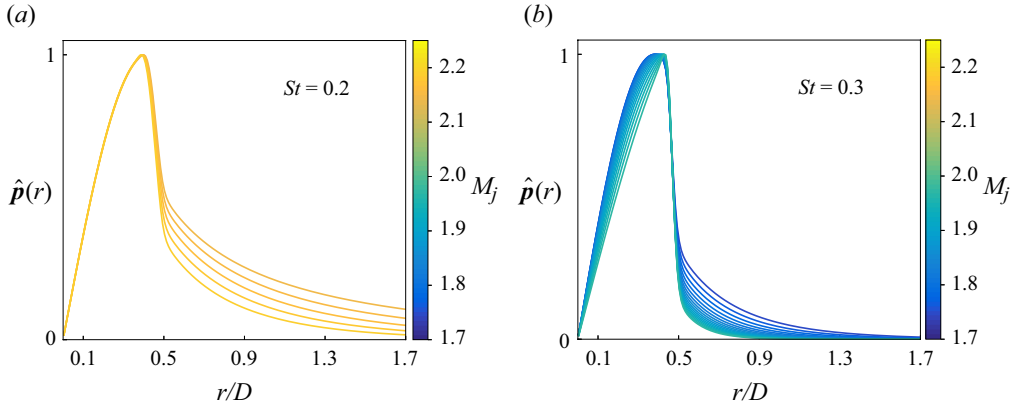


Figure 21. Eigenfunction of the GJM found at $St = 0.2$ (*a*) and $St = 0.3$ (*b*).

the base flow would be necessary if a precise resonance prediction is needed. We refer the reader to Chow & Chang (1975) or Li & Ben-Dor (1998) for this purpose.

The use of a parallel isobaric flow model might also be cause of this inadequation between the model and the observations. Indeed, the flow exiting the nozzle is not parallel. For example, as for underexpanded jets, the shock-cell network modulates the mean flow in the axial direction and it has been shown to be an important feature in screeching jets (Nogueira *et al.* 2022).

Despite these limitations, the analysis conducted in this study revealed that the topology of the flow exiting a convergent divergent nozzle does support the necessary instability waves to produce a resonance (i.e. downstream K–H waves and upstream GJM).

4. Conclusions and perspectives

In this article, the linear dynamics of inviscid annular supersonic jets, similar to those encountered in the exhaust of a converging–diverging nozzle, was explored. The aim was to provide insights into the physical origins of tonal dynamics, observed in very limited expansion regimes in experiments (Baars *et al.* 2012; Jaunet *et al.* 2017*b*), and possibly responsible for unsteady side-loads (Martelli *et al.* 2020; Bakulu *et al.* 2021). The focus was, therefore, put on the first azimuthal Fourier mode of flow fluctuations, which is the

https://doi.org/10.1017/jfm.2025.156 Published online by Cambridge University Press

only one responsible for off-axis loads in axisymmetric nozzles. The dynamical properties of such fluctuations were computed on base flows with varying inner mixing layer radial positions or varying mixing layer thicknesses. Finally, the effect of a variable expansion regime, i.e. an increase in NPR, which the flow can encounter during the start-up of an engine, was explored.

As expected from the shape of the base flows, two unstable K–H waves were found in all cases. The K–H wave supported by the outer mixing layer has, for most of the time, been found to be more unstable than the inner one. This is coherent with the differences in velocity gradients in the two mixing layers. Each of the associated eigenfunctions shows a maximum at the location of the mixing layers, which is typical of the K–H wave. The eigenfunctions of the outer K–H waves never showed significant changes as function of the variation of flow parameters. On the contrary, the inner K–H eigenfunctions were shown to be more affected by base flow changes. Their structure can show a secondary peak at the location of the outer mixing layer and, more importantly, they seem to have a more pronounced signature outside the jet than the outer K–H wave. The fact that the inner K–H wave has support outside the jet must be noted as it allows this wave to exchange energy with external acoustics or upstream travelling waves. It underpins the fact that the inner mixing layer, emanating from the Mach disk triple point, is a probable source of instability in the resonance observed in convergent–divergent nozzles, as conjectured in Jaunet *et al.* (2017) and observed numerically by Bakulu *et al.* (2021).

The article purposely took interest in describing the GJM structure and dynamical characteristics as they have recently been shown to be responsible for the feedback process in jet resonances (see Edgington-Mitchell *et al.* (2022); Varé & Bogey (2022) for recent references). The most striking result of the current study is the robustness of the GJM: they were found in all cases and their eigenfunctions were shown to be very poorly sensitive to the base flow parameters tested. This is a clear indication that, whenever a jet flow is considered, one must pay attention to these waves as they could be involved in the dynamics. In our case, the dispersion relation and the existence of the upstream-travelling wave depended strongly on the inner mixing layer position inside the jet but rather poorly on the mixing layer thicknesses The latter result suggests that they could be observed further downstream in an exhausting jet that diffuses into the surroundings.

Finally, a simplified base-flow model was derived to evaluate the stability properties of the flow with varying NPR but arbitrarily fixed mixing layer thicknesses. Like the hypothetical base flows used at the beginning of the study, two K–H modes and numerous GJM could be identified in the eigenspectra of the analysis, with characteristics found in line with previous results. Interestingly, we observed that the inner K–H wave has a rather small growth rate at low Mach number (NPR) that suddenly increases when the Mach number at which resonances were experimentally observed is reached. Although this can be fortuitous, this is yet another indication that we have possibly pinpointed the correct waves at play in the resonances in such flows and that the inner mixing layer is of great importance in the dynamics of such flows.

Although the results of this study revealed an interesting feature of the dynamics of annular supersonic jets, we must recall that an important number of simplifications were made to be able to conduct the analysis. These assumptions are very likely to be the reason why the prediction of resonance frequency, as was done in the screeching jet case, was not possible. This suggests the need for improvement of the base flow modelling, by considering a more representative control volume (Li & Ben-Dor 1998), consideration of the influence of the nozzle walls or even the relaxation of the parallel flow assumption by the use of a global stability analysis.

https://doi.org/10.1017/jfm.2025.156 Published online by Cambridge University Press

Declaration of interests. The authors report no conflict of interest.

Appendix A

A.1 *Mass conservation*

Applying mass conservation on a control volume delimited by the nozzle throat and the attached flow, as presented in grey in figure 3, we can write

$$\rho_* U_* D_c^2 = \rho_i U_i D_i^2 + \rho_a U_a (D_e^2 - D_i^2), \tag{A1}$$

where $(\cdot)_*$ denotes sonic variables at the throat.

Using perfect gas relations and introducing the speed of sound, such that $U = aM = \sqrt{\gamma r T} \cdot M$ and recalling that $M_* = 1$, we have

$$\frac{P^*}{rT^*} a^* M^* {D_c}^2 = \frac{P_i}{rT_i} a_i M_i D_i^2 + \frac{P_i}{rT_i} a_i M_i (D_e^2 - D_i^2) \tag{A2}$$

$$\frac{P^*}{\sqrt{rT^*}} {D_c}^2 = \frac{P_i}{\sqrt{rT_i}} M_i D_i^2 + \frac{P_a}{\sqrt{rT_a}} M_a (D_e^2 - D_i^2). \tag{A3}$$

Then, using isentropic relation to link static and total variables, we obtain

$$\left(1 + \frac{\gamma - 1}{2}\right)^{-\frac{\gamma+1}{2(\gamma-1)}} \frac{P_{t0}}{\sqrt{T_{t0}}} D_c^2 = \frac{P_i}{\sqrt{T_i}} \mathcal{M}_i D_i^2 + \frac{P_a}{\sqrt{T_a}} \mathcal{M}_a (D_e^2 - D_i^2). \tag{A4}$$

Choosing $P_a = P_i = P_\infty$, we can further simplify the mass conservation equation to

$$\left(1 + \frac{\gamma - 1}{2}\right)^{-\frac{\gamma+1}{2(\gamma-1)}} \frac{P_{t0}}{P_\infty} D_c^2 = D_i^2 \mathcal{M}_i \sqrt{1 + \frac{\gamma - 1}{2} \mathcal{M}_i^2} + (D_e^2 - D_i^2) \mathcal{M}_a \sqrt{1 + \frac{\gamma - 1}{2} \mathcal{M}_a^2}, \tag{A5}$$

which can be written in the more compact form presented in the document,

$$\beta_m \frac{D_c^2}{D_e^2} = (\mu_i - \mu_a) \frac{D_i^2}{D_e^2} + \mu_a, \tag{A6}$$

where

$$\mu_{i,a} = \mathcal{M}_{i,a} \sqrt{1 + \frac{\gamma - 1}{2} \mathcal{M}_{i,a}^2} \tag{A7}$$

$$\beta_m = \left(1 + \frac{\gamma - 1}{2}\right)^{-\frac{\gamma+1}{2(\gamma-1)}} \frac{P_{t0}}{P_\infty}. \tag{A8}$$

A.2 *Momentum conservation*

Now, considering the momentum conservation along the axial direction on the same control volume, and neglecting body and viscous forces, leads to

$$\gamma P_* {\mathcal{M}_*}^2 D_c^2 + P_* D_c^2 = \gamma P_i \mathcal{M}_i^2 D_i^2 + P_i D_i^2 + \gamma P_a \mathcal{M}_a^2 (D_e^2 - D_i^2) + P_a (D_e^2 - D_i^2) - F_w, \tag{A9}$$

https://doi.org/10.1017/jfm.2025.156 Published online by Cambridge University Press

where F_w represents the pressure forces acting on the nozzle wall. Using isentropic relations, isobaric assumption (as for the mass conservation) and rearanging provides

$$(1+\gamma)\left(1+\frac{\gamma-1}{2}\right)^{\frac{-\gamma}{\gamma-1}}\frac{P_{t0}}{P_\infty}D_c^2-\frac{F_w}{P_\infty}=D_i^2(\gamma\mathcal{M}_i^2+1)+D_e^2(\gamma\mathcal{M}_a^2+1)-D_i^2(\gamma\mathcal{M}_a^2+1), \tag{A10}$$

which can be written in the more compact form

$$\beta_q\frac{D_c^2}{D_e^2}-\frac{F_w}{P_\infty}=\gamma\frac{D_i^2}{D_e^2}\left(\mathcal{M}_i^2-\mathcal{M}_a^2\right)+\left(\gamma\mathcal{M}_a^2+1\right), \tag{A11}$$

where

$$\beta_q=(1+\gamma)\left(1+\frac{\gamma-1}{2}\right)^{\frac{-\gamma}{\gamma-1}}\frac{P_{t0}}{P_\infty}. \tag{A12}$$

From the latter equation, we get an analytical expression for D_i^2,

$$D_i^2=D_e^2\frac{1}{\gamma\left(\mathcal{M}_i^2-\mathcal{M}_a^2\right)}\left[\beta_q D_c^2-\frac{F_w}{P_\infty}-\left(\gamma\mathcal{M}_a^2+1\right)\right], \tag{A13}$$

which can be plugged into the mass conservation equation leading to the equation for the annular Mach number presented in the document,

$$\frac{\mu_i-\mu_a}{\gamma\left(\mathcal{M}_i^2-\mathcal{M}_a^2\right)}\left[\beta_q D_c^2-\frac{F_w}{P_\infty}-\left(\gamma\mathcal{M}_a^2+1\right)\right]+\mu_a-\beta_m=0, \tag{A14}$$

where

$$\begin{aligned}\mu_{i,a}&=\mathcal{M}_{i,a}\sqrt{1+\frac{\gamma-1}{2}\mathcal{M}_{i,a}^2}\\ \beta_m&=\left(1+\frac{\gamma-1}{2}\right)^{-\frac{\gamma+1}{2(\gamma-1)}}\frac{P_{t0}}{P_\infty}\\ \beta_q&=(1+\gamma)\left(1+\frac{\gamma-1}{2}\right)^{\frac{-\gamma}{\gamma-1}}\frac{P_{t0}}{P_\infty}.\end{aligned} \tag{A15}$$

References

Baars, W.J., Tinney, C.E., Ruf, J.H., Brown, A.M. & McDaniels, D.M. 2012 Wall pressure unsteadiness and side loads in overexpanded rocket nozzles. *AIAA J.* **50** (1), 61–73.

Bakulu, F., Lehnasch, G., Jaunet, V., Goncalves da Silva, E. & Girard, S. 2021 Jet resonance in truncated ideally contoured nozzles. *J. Fluid Mech.* **919**, A32.

Bhat, T. & Seiner, J. 1993 The effect of velocity profiles on supersonic jet noise. In *15th Aeroacoustics Conference*, pp. 4410. AIAA.

Chow, W.L. & Chang, I.S. 1975 Mach reflection associated with over-expanded nozzle free jet flows. *AIAA J.* **13** (6), 762–766.

Dahl, M.D. & Morris, P.J. 1997*a* Noise from supersonic coaxial jets, part 1: mean flow predictions. *J. Sound Vib.* **200** (5), 643–663.

Dahl, M.D. & Morris, P.J. 1997*b* Noise from supersonic coaxial jets, part 3: inverted velocity profile. *J. Sound Vib.* **200** (5), 701–719.

Dahl, M.D. & Morris, P.J. 1997*c* Noise from supersonic coaxial jets, part 2: normal velocity profile. *J. Sound Vib.* **200** (5), 665–699.

Deck, S. 2009 Delayed detached eddy simulation of the end-effect regime and side-loads in an overexpanded nozzle flow. *Shock Waves* **19** (3), 239–249.

https://doi.org/10.1017/jfm.2025.156 Published online by Cambridge University Press

DECK, S. & NGUYEN, A.T. 2004 Unsteady side loads in a thrust-optimized contour nozzle at hysteresis regime. *Aiaa J.* **42** (9), 1878–1888.

DOSANJH, D.S., ABDELHAMID, A.N. & YU, J.C. 1969 Noise reduction from interacting coaxial supersonic jet flows. *NASA SP* **207**, 63–101.

DOSANJH, D.S., YU, J.C., ABDELHAILIID, A.M.R.N. 1971 Reduction of noise from supersonic jet flows. *AIAA J.* **9** (12), 2346–2353.

DUMNOV, G. 1996 Unsteady side-loads acting on the nozzle with developed separation zone. In *32nd Joint Propulsion Conference and Exhibit*, pp. 1–8. AIAA.

EDGINGTON-MITCHELL, D. 2019 Aeroacoustic resonance and self-excitation in screeching and impinging supersonic jets–a review. *Intl J. Aeroacoust.* **18** (2–3), 118–188.

EDGINGTON-MITCHELL, D., JAUNET, V., JORDAN, P., TOWNE, A., SORIA, J. & HONNERY, D. 2018 Upstream-travelling acoustic jet modes as a closure mechanism for screech. *J. Fluid Mech.* **855**, R1.

EDGINGTON-MITCHELL, D., LI, X., LIU, N., HE, F., WONG, T.Y., MACKENZIE, J. & NOGUEIRA, P. 2022 A unifying theory of jet screech. *J. Fluid Mech.* **945**, A8.

GOJON, R., BOGEY, C. & MIHAESCU, M. 2018 Oscillation modes in screeching jets. *AIAA J.* **56** (7), 2918–2924.

HADJADJ, A. & ONOFRI, M. 2009 Nozzle flow separation. *Shock Waves* **19** (3), 163–169.

JAUNET, V., ARBOS, S., LEHNASCH, G. & GIRARD, S. 2017 Wall pressure and external velocity field relation in overexpanded supersonic jets. *AIAA J.* **55** (12), 4245–4257.

JAUNET, V., MANCINELLI, M., JORDAN, P., TOWNE, A., EDGINGTON-MITCHELL, D.M., LEHNASCH, G. & GIRARD, S. 2019 Dynamics of round jet impingement. In *25th AIAA/CEAS Aeroacoustics Conference*, pp. 2769. AIAA.

JORDAN, P. & COLONIUS, T. 2013 Wave packets and turbulent jet noise. *Annu. Rev. Fluid Mech.* **45** (1), 173–195.

JORDAN, P., JAUNET, V., TOWNE, A., CAVALIERI, A.V.G., COLONIUS, T., SCHMIDT, O. & AGARWAL, A. 2018 Jet–flap interaction tones. *J. Fluid Mech.* **853**, 333–358.

LI, H. & BEN-DOR, G. 1998 Mach reflection wave configuration in two-dimensional supersonic jets of overexpanded nozzles. *AIAA J.* **36** (3), 488–491.

MANCINELLI, M., JAUNET, V., JORDAN, P. & TOWNE, A. 2019 Screech-tone prediction using upstream-travelling jet modes. *Exp. Fluids* **60** (1), 22.

MANCINELLI, M., JAUNET, V., JORDAN, P. & TOWNE, A. 2021 A complex-valued resonance model for axisymmetric screech tones in supersonic jets. *J. Fluid Mech.* **928**, A32.

MANCINELLI, M., MARTINI, E., JAUNET, V., JORDAN, P., TOWNE, A. & GERVAIS, Y. 2023 Reflection and transmission of a Kelvin–Helmholtz wave incident on a shock in a jet. *J. Fluid Mech.* **954**, A9.

MARTELLI, E., SACCOCCIO, L., CIOTTOLI, P.P., TINNEY, C.E., BAARS, W.J. & BERNARDINI, M. 2020 Flow dynamics and wall-pressure signatures in a high-Reynolds-number overexpanded nozzle with free shock separation. *J. Fluid Mech.* **895**, A29.

MICHALKE, A. 1984 Survey on jet instability theory. *Prog. Aerosp. Sci.* **21**, 159–199.

NAVE, L.H. & COFFEY, G.A. 1973 Sea level side loads in high-area-ratio rocket engines. In *9th Propulsion Conference*. AIAA.

NOGUEIRA, P.A.S., JORDAN, P., JAUNET, V., CAVALIERI, A.V.G., TOWNE, A. & EDGINGTON-MITCHELL, D. 2022 Absolute instability in shock-containing jets. *J. Fluid Mech.* **930**, A10.

SCHMIDT, O.T., TOWNE, A., COLONIUS, T., CAVALIERI, A.V.G., JORDAN, P. & BRÈS, G.A. 2017 Wavepackets and trapped acoustic modes in a turbulent jet: coherent structure eduction and global stability. *J. Fluid Mech.* **825**, 1153–1181.

SCHMUCKER, R.H. 1973*a* Flow process in overexp*a*nded chemical rocket nozzles part 1: flow separation. *NASA Tech. Mem*. NASA-TM-77396. NASA.

SCHMUCKER, R.H. 1973*b* Flow process in overexpanded chemical rocket nozzles part 2 : side loads due to asymetric separation. *NASA Tech. Mem*. NASA-TM-77395. NASA.

SCHMUCKER, R.H. 1973*c* Flow process in overexpanded chemical rocket nozzles part 3: methods for the aimed flow separation and side load reduction. *NASA Tech. Mem*. NASA-TM-77048. NASA.

STARK, R.H. 2005 Flow separation in rocket nozzles, a simple criteria. In *41st AIAA/ASME/SAE/ASEE Joint Propulsion Conference & Exhibit*. AIAA.

TAM, C.K.W. 1972 On the noise of a nearly ideally expanded supersonic jet. *J. Fluid Mech.* **51** (1), 69–95.

TAM, C.K.W. 1991 Broadband shock-associated noise from supersonic jets in flight. *J. Sound Vib.* **151** (1), 131–147.

TAM, C.K.W. & HU, F.Q. 1989 On the three families of instability waves of high-speed jets. *J. Fluid Mech.* **201**, 447–483.

https://doi.org/10.1017/jfm.2025.156 Published online by Cambridge University Press

TAM, C.K.W. & TANNA, H.K. 1985*a* Shock associated noise of inverted-profile coannular jets, part ii: condition for minimum noise. *J. Sound Vib.* **98** (1), 115–125.

TAM, C.K.W. & TANNA, H.K. 1985*b* Shock associated noise of inverted-profile coannular jets, part iii: shock structure and noise characteristics. *J. Sound Vib.* **98** (1), 127–145.

TANNA, H.K., BROWN, W.H. & TAM, C.K.W. 1985 Shock associated noise of inverted-profile coannular jets, part i: experiments. *J. Sound Vib.* **98** (1), 95–113.

TANNA, H.K., TESTER, B.J. & LAU, J.C. 1979 The noise and flow characteristics of inverted-profile coannular jets. *NASA Tech. Rep.* NASA-CR-158995. NASA.

TARSIA MORISCO, C., ROBINET, J,-C., HERPE, J & SAUCEREAU, D. 2023 Impinging shear layer instability in over-expanded nozzle dynamics. *Phys. Fluids* **35**, 116118.

TOWNE, A., CAVALIERI, A.V.G., JORDAN, P., COLONIUS, T., SCHMIDT, O., JAUNET, V. & BRÈS, G.A. 2017 Acoustic resonance in the potential core of subsonic jets. *J. Fluid Mech.* **825**, 1113–1152.

TREFETHEN, L.N. 2000 *Spectral Methods in MATLAB*. SIAM.

VARÉ, M. & BOGEY, C. 2022 Generation of acoustic tones in round jets at a mach number of 0.9 impinging on a plate with and without a hole. *J. Fluid Mech.* **936**, A16.

YU, J.C. & DOSANJH, D.S. 1971 Noise field of coaxial interacting supersonic jet flows. In *9th Aerospace Sciences Meeting*. AIAA.

https://doi.org/10.1017/jfm.2025.156 Published online by Cambridge University Press